Carbonates and Evaporites (2020) 35:106
https://doi.org/10.1007/s13146-020-00637-x

ORIGINAL ARTICLE

Discovery of spherulitic dahllite associated with carbonates at Hamadat phosphorite mine, Qusseir, Central Eastern Desert, Egypt

Esmat A. Abou El-Anwar[1] · Hamed S. Mekky[1] · Said H. Abd El Rahim[1]

Accepted: 12 September 2020 / Published online: 6 October 2020

Abstract

Microscopical and mineralogical studies reveal first recorded spherulitic dahllite ($3Ca_3(PO_4)_2\ Ca\ CO_3$) in the phosphorite rocks associated with carbonate rocks of Hamadat Mines (Duwi Formation) at Qusier area, Central Eastern Desert, Egypt. Mineralogically, the phosphatic rocks of Hamadat Mines are mainly consisting of fluor-apatite, dahllite, dolomite, calcite, quartz and pyrite. Petrographically, the studied dahllite in Hamadat Mines are authigenic in origin. Genetically, spherulitic dahllite at Hamadat Mines (Duwi Formation) in Qusier area is resulting from diagenesis processes; dolomitization and the re-crystallization process. Geochemical analysis of trace, rare earth elements and the petrogaphical is indicated that the phosphatic rocks are deposited under oxic to anoxic condition. Dolomitization process plays an important role in the concentration of trace and rare earth elements in the phosphatic rocks at Hamadat Mine. Dahllite layer has a relatively higher content in most of rare earth and some of the trace elements than those in the phosphate layer, which reveal that dahllite structure may be having the ability to scavenging them than the phosphatic construction. The chemical index of alteration (CIA), trace elements and La/Ce ratios pointed out that these phosphatic rocks were of hydrogenous origin deposited in cold and dry climate during low weathering. Finally, the hydroxial-apatite can be prepared to be used as a natural row material in the biological industry according to the chemical composition.

Keywords Dahllite · Hamadat mines · Trace elements · Rare earth elements

Introduction

The chosen area in Hamadat Mines is located at longitudes 34° 11′ 25″- 34° 11′ 32″ E and latitudes 26° 02′ 55″—26° 03′ 21″ N, which is located 8 km south of the Gebel Duwi mines, 15 km from Qusseir—Qaft, Asphalt Road to west.

Generally, Dahllite ($3Ca_3(PO_4)_2\ Ca\ CO_3$); is a carbonate–apatite mineral. Also, it can defined as biological apatite (Dorozhkin 2010). It typically occurs in phoshorite rocks. It has different origins such as weathered bones or coprolites (Sanz et al. 2015). The concentric spherulitic dahllite can reach up to 3 cm in diameter.

Sedimentary marine phosphorites representing the world's main source of phosphorus fertilizers, were deposited sporadically along continental and ocean basin margins. Egyptian phosphorites represent a part of the Tethyan phosphogenic province. They form a belt stretching from the Red Sea across the Nile Valley into the Western Desert. They occur interbedded with a siliciclastic facies (shales and sandstones) in the lower part of the stratigraphic sequence and/or a carbonate facies (oyster limestone, marl and chert) in the upper part (Said 1990). The phosphorite beds intercalated with the siliciclastic facies represented the early transgressive stage, which is characterized by the dominance of detrital input (Said 1990). High detrital influx indicated to the southern coastal of Egypt acted as sediment traps in areas. In addition, the fluvial and tidal currents accounted for the concentration of phosphate particles within this facies (Germann et al. 1987). They, also mentioned that during the deposition of the upper stratigraphic phosphorite sequence associated with the carbonate facies at the shallow shelf condition increased it was interrupted by the build-up of oyster reefs which protected the depositional area from terrestrial input (Germann et al. 1987). The Duwi Formation deposited at the initial stage of the late Cretaceous marine transgression in Egypt (Baioumy and Tada 2005). Phosphorites display a broad difference in colour, grain size and friability

✉ Esmat A. Abou El-Anwar
abouelanwar2004@yahoo.com

[1] Geological Sciences Department, National Research Centre, Dokki, Giza, Egypt

in the Duwi Formation. The grain size varies from coarse to fine sand size, with the majority being medium grained. Colour of the phosphorites varies widely from grey, yellow to brown.

Abou El-Anwar et al. (2017) studied the mineralogical and geochemical characters of the phosphate rocks of the Duwi Formation of Geble Duwi Mine in Quseir-Safaga area to infer the paleo-weathering and provenance of the sources. Also, they mentioned the importance in the assessment of possible radiological hazards to human health; due to the presence of uranium in the apatite structure.

The Lower phosphatic member (Campanian, Upper Cretaceous), Duwi Formation, is an important rock unit resulting in relatively high enrichment of heavy metals and U content in south Esna, at the western side of the Nile Valley (Abou El-Anwar 2019). In addition, she mentioned that U contents were associated with the heavy metals and trace elements during the chemical weathering under oxic conditions. Also, she concluded by the same author that the phosphatic rocks were in south Esna deposited under anoxic reducing marine environments coupled with hydrothermal solutions.

The aim of this study is to interpret the mineralogical, petrographical and the geochemical behaviour of some trace and rare earth elements in the phosphorites associated with carbonate at Hamadat Mines, to infer their depositional environment and genesis as well as to evaluate their economic potentialities. Fifteen representative samples were collected from the phosphatic rocks from Hamadat mines in the south part of the Qusseir.

Geological setting

The sedimentary phosphatic rocks (Upper Cretaceous—Eocene) originated in marine environments. The Mediterranean phosphatic rocks such as in Egypt, Algeria, Tunisia, Jordan, Syria, Saudi Arabia, Spain,…etc., are deposited in the ancient Tethes Sea(Sengul et al. 2006). In Egypt, the phosphatic rocks of Duwi Formation are located in the Nile-Valley, the Red Sea Coast, Abu Tartur plateau and Sinai. The Duwi Formation in the Qusseir-Safaga region is conformably underlain by the Qusseir variegated shales and overlain by the Dakhla shales (Said 1990). Duwi Formation in Egypt represents the early stage of the Late Cretaceous marine transgression. It was classified into four members according to its lithology (Baioumy and Tada 2005) subdivided the Duwi Formation in the studied area into four members (Fig. 2). The lower member that ranges from 35 to 50 m consists of yellowish-grey laminated, silty claystone, greyish-yellow laminated, siliciclastic sandstone, grey, laminated shale, and yellowish-grey and finely intercalated with thin beds of phosphorite, marl, oyster fragment-rich calcarenite. The middle member that ranges in thickness from 5 to 12 m is composed of soft, yellowish-grey laminated shales that are intercalated with 2–25 cm of yellowish-grey, massive, hard, coarse-grained, siliceous, phosphorites. The upper member is made up of 3–30 m of yellowish-grey, oyster fragments-rich calcarenite intercalated of siltstone, shale, chert, and phosphorite. The uppermost member is 1.2–5 m thick and consists of grey, massive, coarse-grained phosphorite intercalated with 80 cm thin laminated black shale and overlain by greyish brown shales. Most of the phosphate beds appear as massive rocks. Their thickness is up to tens of centimeters.

The selected area is represented by Hamadat Mines (Figs. 1 and 2). They occur at the upper Member of Duwi Formation in south Qusseir region (Fig. 3). Phosphatic rocks in these mines are formed as horizontal layers, which extend to several kilometers. These phosphatic beds are deposited above a layer of black shales. They vary in thickness up to 2.5 m. The phosphatic rocks consist mainly of two layers in the studied area. Generally, phosphorite rocks (spherulitic dahllite and collophane), associated with carbonates (calcite and dolomite) at studied area of Hamadat Phosphorite Mines. The characteristic top layer (Dahllite) was pale grey color and highly fossilifrous and up to 1 m in thickness. This layer as associated with white carbonate rocks and this rock is crossed by folded veinlets due to subsequent deformations (Fig. 4). The lower layer (Phosphatic) was yellowish in color and thickness up to 2 m (very thick bed) (Fig. 4). These mines represent the extension of the phospharite beds of Gebel Duwi mines south Qusseir.

Sampling and methodology

Seven samples (S. Nos. 9–15) were from the top bed and the other eight (S. Nos. 1–8) were collected from the lower bed in horizontal direction. The upper was bed about 60 cm and the other lower range from 2 to 3 m in thickness. Mineralogically, selected four samples were investigated by the X-ray technique at the Egyptian Mineral Resources Authority (Dokki, Egypt) using a PAN analytical X-Ray Diffraction equipment model X′Pert PRO with Secondary Monochromator, Cu-Radiation ($\lambda = 1.542$ Å) at 45 K.V., 35 M.A. and scanning speed 0.02°/sec. were used. The diffraction charts and relative intensities are obtained and compared with ICDD files. The morphology and the size of the synthesized samples were characterized via SEM, coupled with energy-dispersive spectroscopy EDAX, (SEM Model Quanta FEG 250) of the selected samples were carried out in the National Research Center laboratories. Eight samples were selected to determine the chemical composition using Axios Sequential WD-XRF Spectrometer, Analytical 2005 in the National Research Center laboratories, with reference to

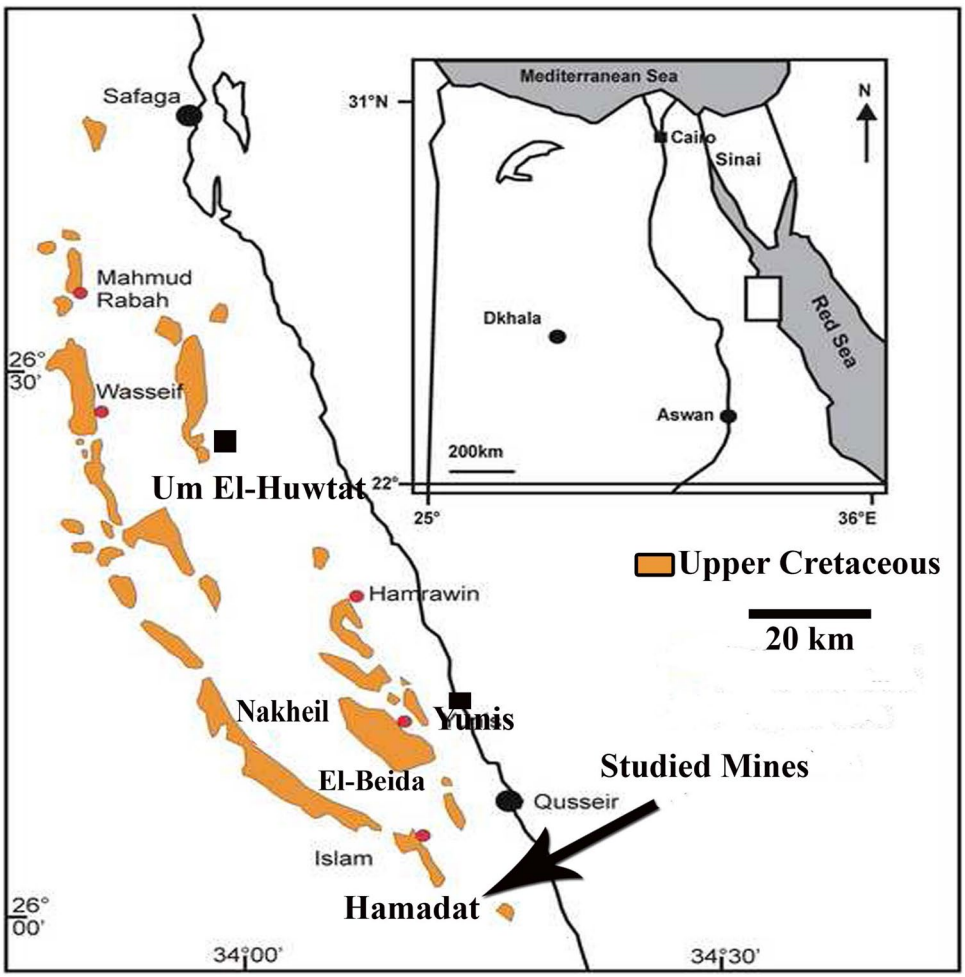

Fig.1 Location map of the studied Hamadat Mines

the ASTM E 1621 standard guide for elemental analysis by wavelength dispersive X-ray fluorescence spectrometer and ASTM D 7348 standard test methods for loss on ignition (LOI) on solid combustion.

Mineralogy

The X-ray diffraction analysis of the studied bulk samples of the lower beds revealed that they are mainly composed of calcite, fluor-apatite, dolomite, quartz and pyrite. Meanwhile, the upper bed consists of dahllite, dolomite, calcite and quartz (Fig. 5).

SEM and EDX examination of the phosphatic samples were recorded P, Si and Ca (~ 9, 7 and 16%; respectively) showing maceral occurs as roded-shaped and accumulated parallel to the lamination (Fig. 6) and represents an authochthonous type (Nowak 2007 and Abou El-Anwar et al. 2019a). SEM and EDX of Dahllite sample was recorded Mg, Si, Na and Cl (4.7, 7.3, 5.8 and 1.3%; respectively), showing dolomite and halite crystals are scattered in phosphatic matrix (Fig. 7).

Petrographical study

The detailed microscopic examinations indicate that the carbonate rocks are essentially composed of the mineral dolomite, calcite, few magnesite, in addition to opaques, and quartz grains in decreasing order of abundance. The associated phosphate minerals are mainly represented by collophane [amorphous or mineraloid calcium carbonate-phosphate] and spherulitic dahllite [3 Ca_3 $(PO^4)_2$ $CaCO_3$], according to their order of the paragenetic sequence. Hence the order of the paragenetic sequence of the whole described rock components are as follows: carbonates (calcite, dolomite), followed by collophane and lastly spherulitic dahllite.

Phosphatic rocks

(1) Collophane

Microscopically, collophane is an amorphous or mineraloid calcium carbonate-phosphate. It is brown subidiomorphic to hypidiomorphic fine to coarse grains and aggregates, brown pellets, spheroids, ovoids are also commonly observed

Fig. 2 General view of the studied phosphatic Hamadat Mines

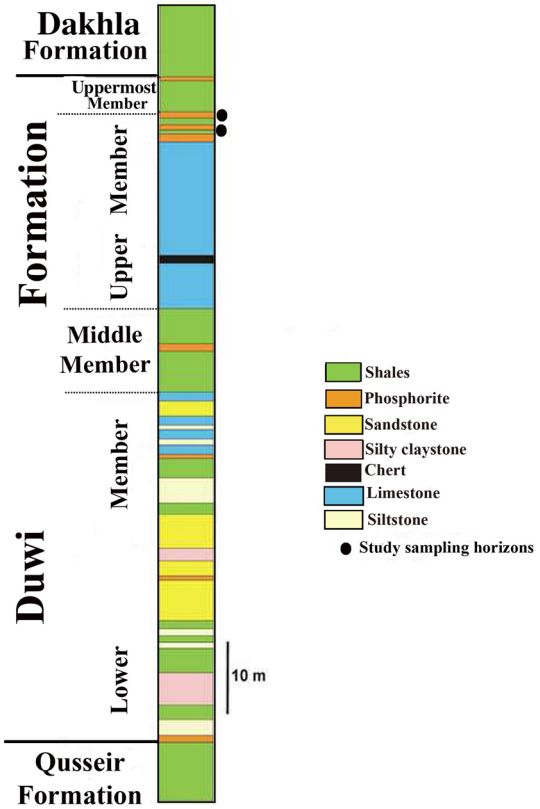

Fig. 3 Stratigraphic columnar section of the Duwi Formation in the Red Sea area showing the stratigraphic site of the black shale beds (after Baioumy and Tada 2005)

(Figs. 8, 10, 12, 14 and 16). Collophane appears isotropic under crossed Nichols (Figs. 9, 11, 13, 15 and 19). Collophane encloses some rock fragments of the carbonates (Figs. 10 and 11). Carbonates were later on corroded and embayed by the collophane mineral, where collophane is growing at the expense of the carbonates. The boundaries of collophane are convex towards carbonates (Figs. 8, 9, 10, 11, 12, 13, 14 and 15). Lastly, microscopic studies revealed that the spherulitic dahllite was invading and replacing collophane as well as carbonates (calcite, dolomite, few magnesite), where the spherulitic dahllite is growing at the expense of the collophane as well as carbonates (Figs. 12, 13, 14, 15, 16, 17, 18 and 19).

(2) Dahllite: ($3\ Ca_3\ (PO_4)_2\ CaCO_3$)

Discovery of spherulitic dahllite structure is microscopically recorded for the first time by the present authors in the phosphorite of Hamadat Mines (Duwi Formation) in Qusier area, (cf. Abou El-Anwar et al. 2017). Dahllite (carbonate-apatite mineral) occurs as colourless to pale brown spherulites (Figs. 12, 14, 16 and 18). It commonly forms plumose fibers of the spherulitic structure. It also commonly exhibits subradiating fibrous structure (cf. Lacroix 1910; Rogers

Fig. 4 Hand specimen of rock sample of phosphorite (spherulitic dahllite and collophane) associated with carbonates (calcite and dolomite) showing spherulitic dahllite structure. Note the rock is crossed by folded veinlets due to subsequent deformations. These veinlets are filled by spherulitic dahllite. Hamadat Phosphorite Mines

and Kerr 1942; Abou El-Anwar et al. 2017). It is sometimes fine-grained anhedral crystal aggregates of the spherulitic structure. It exhibits moderate relief and bluish gray to white of the first order interference colours (Figs. 15, 17 and 19). It exhibits parallel extinction, whereas cross sections appear

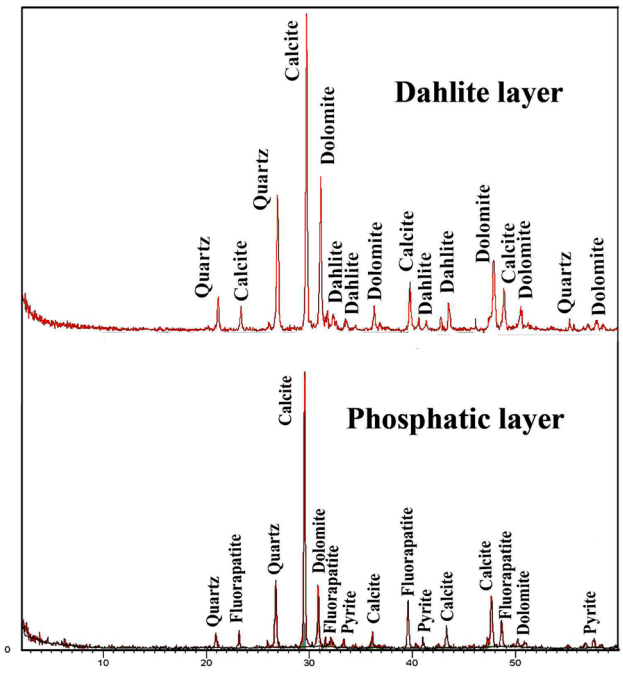

Fig. 5 X-ray diffractograms for the phosphatic and dahllite rocks of the studied Hamadat Mines

dark between crossed Nichols (Hexagonal Crystal System). Most probably, the dahllite has been formed by the gradual crystallization of the collophane (amorphous or mineraloid calcium carbonate-phosphate) and by the migration of some of the calcium phosphate (Rogers 1912, 1924; Eitel 1924 and Abou El-Anwar et al. 2017). Also, the dahllite may have formed by the gradual crystallization and replacement of the collophane as well as carbonates (calcite, dolomite, few magnesite). Hence, the dahllite contains inclusions of collophane (brown grains, pellets, spheroids, ovoids which appear isotropic between crossed Nichols) as well as carbonates. Furthermore, dahllite contains inclusions of pyrite (FeS_2) which appears opaque of subhedral cubes and anhedral grains.

Framboidal pyrite is also commonly observed where pyrite occurs as framboids (Figs. 12, 13, 14, 15, 16, 17, 18 and 19). Pseudomorphosed framboidal pyrite formed as authigenic. Framboidal pyrite is precipitated in some voids of the bone fragments. The framboids (4.5 µm) are indicating the occurrence under shallow anoxic reducing conditions which confirms with the chemical study by Abou El-Anwar and Sadek (2008); Abou El-Anwar 2017 and Abou El-Anwar et al. (2014 and 2017). Pyrite as spheres may be a sign indicating shallow marine water (Schieber and Baird 2001). Lastly, the petrographic study indicated that the spherulitic dahllite invaded and replaced collophane as well as carbonates (calcite, dolomite, few magnesite), whereas the spherulitic dahllite is growing at the expense of the collophane as well as carbonate rocks, (Figs. 12 13, 14, 15, 16, 17, 18 and 19). Therefore, the dahllite commonly occurs as rims around collophane and carbonates, as well as pseudomorphs after the collophane and carbonates in the phosphorite (cf. Abou El-Anwar 2019). The phosphorite is crossed by folded microveinlets due to subsequent deformations. These microveinlets are filled by spherulitic dahllite and/or framboidal pyrite (Figs. 12, 14, 16 and 18). It is commonly associated with francolite, collophane, and other phosphatic minerals in the phosphorite.

The spherulitic dahllite structure in the phosphorite at Hamadat Mines (Duwi Formation) in Qusier area (Late Cretaceous) may be similar to, and comparable with those occurring Thermopolis Formation (Upper Cretaceous), in Cody, Wyoming, United States (Eitel 1924). Also, it is comparable to the phosphatic rocks of Gebel Duwi Mine (Abou El-Anwar et al. 2017).

Carbonate rock

Microscopically, the carbonate rocks are essentially composed of calcite, dolomite, few magnesite, opaques, and quartz. They are cemented by calcareous (developing in clay matrix) and/or phosphatic materials.

(1) Calcite ($CaCO_3$) forms colourless hypidiomorphic fine to coarse grains and aggregates, rhombohedral crystals are also observed (Figs. 8, 10, 12, 14, 16 and 18). It exhibits pastel pink, green, creamy white and pearl grey or bright interference colours of fourth order (Figs. 9, 11, 13 and 17). It is characterized by changes of relief upon rotation of stage, rhombohedral cleavage and lamellar twinning. Calcite was later on corroded and embayed by the collophane mineral, whereas collophane is growing at the expense of the calcite. The boundaries of collophane are convex towards calcite (Figs. 8, 9, 10, 11, 12, 13, 14 and 15). The petrographical investigation shows the spherulitic dahllite as invading and replacing collophane as well as carbonates (calcite, dolomite, few magnesite), where the spherulitic dahllite is going up at the expense of the collophane and carbonates (Figs. 12 13, 14, 15, 16, 17, 18 and 19).

(2) Dolomite [$CaMg(CO_3)_2$] forms colourless hypidiomorphic fine to coarse grains and aggregates, rhombohedral crystals are also commonly observed (Figs. 8, 10, 12, 14, 16 and 18). Dolomite crystals stained with iron oxyhydroxides due to alterations by weathering. It exhibits pastel pink, green, creamy white and pearl grey or bright interference colours of fourth order (Figs. 9, 11, 13, 17 and 19). It is characterized by changes of relief upon rotation of stage, rhombohedral cleavage, lamellar twinning and iron stained. The crystal size up to 80 µm indicates late diagenetic dolomite, which is in agreement with Loukina and Abou El-Anwar 1991, 2006, 2007, 2010, 2011 and 2012. Dolomite was later on corroded and embayed by the

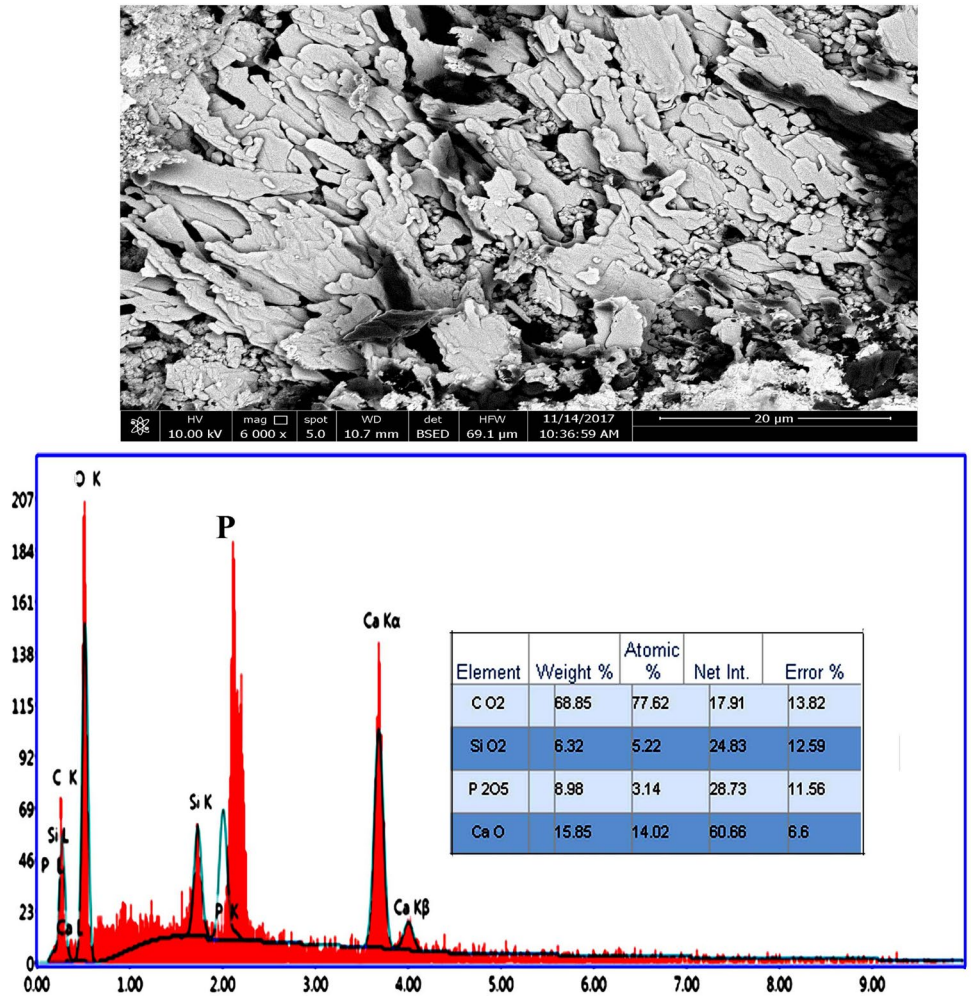

Fig. 6 BSE image and EDX analysis data showing a well-ordered (one direction) maceral of the vertebrates occurs as rod-shaped and accumulated parallel to the lamination at the dahllite layer of the studied Hamadat Mines

collophane mineral, whereas collophane is growing at the expense of the dolomite. The boundaries of collophane are convex towards dolomite (Figs. 8, 9, 10, 11, 12, 13, 14 and 15). Also, the dolomite crystals had the same features of calcite exposed for the spherulitic dahllite (Figs. 12 13, 14, 15, 16, 17, 18 and 19).

(3) Magnesite ($MgCO_3$) occurs as few colourless anhedral to subhedral crystal aggregates. It sometimes, forms porcelain like microcrystalline aggregates (Fig. 10). It shows pastel pink, green, creamy white and pearl grey or bright interference colours of fourth order (Fig. 11). Magnesite was later on corroded and embayed by the collophane mineral (Figs. 10 and 11) as well as spherulitic dahllite, where collophane and spherulitic dahllite are growing at the expense of the magnesite. The boundaries of the collophane and spherulitic dahllite are convex towards magnesite (Figs. 3, 4). Furthermore, the spherulitic dahllite in magnesite was subjected to the same behavior as calcite and dolomite rocks (Figs. 12 13, 14, 15, 16, 17, 18 and 19).

Quartz (SiO_2) forms as colourless, hypidiomorphic and equigranular crystals. It exhibits grey or white first order of interference colours (Figs. 12 13, 14, 15, 16, 17, 18 and 19). It exhibits wavy extinction due to strain.

Opaques are mainly represented by pyrite. Pyrite forms hypidiomorphic to subidiomorphic grains. Later, some of pyrite was oxidized to hematite. Framboidal pyrite is also commonly observed where pyrite occurs as framboids in the matrix (Figs. 12 13, 14, 15, 16, 17, 18 and 19). Framboidal pyrite is extensively pseudomorphosed and formed as authigenic under shallow anoxic reducing conditions.

Genesis of dahllite

Dolomitization process was the most important diagenetic feature that occurred in the study rocks. The sources of Mg may be from sea water, clay materials or vertebrates. This process led to increase Ca ions in water within the phosphatic rocks at Hamadat Mines. Also, re-crystallization process is the main diagenetic feature present in the studied dahllite. Re-crystallization of dahllite involves adding of calcium phosphate to the outstanding crystals. As a result, some trace metal ions in water inside the bone fragments

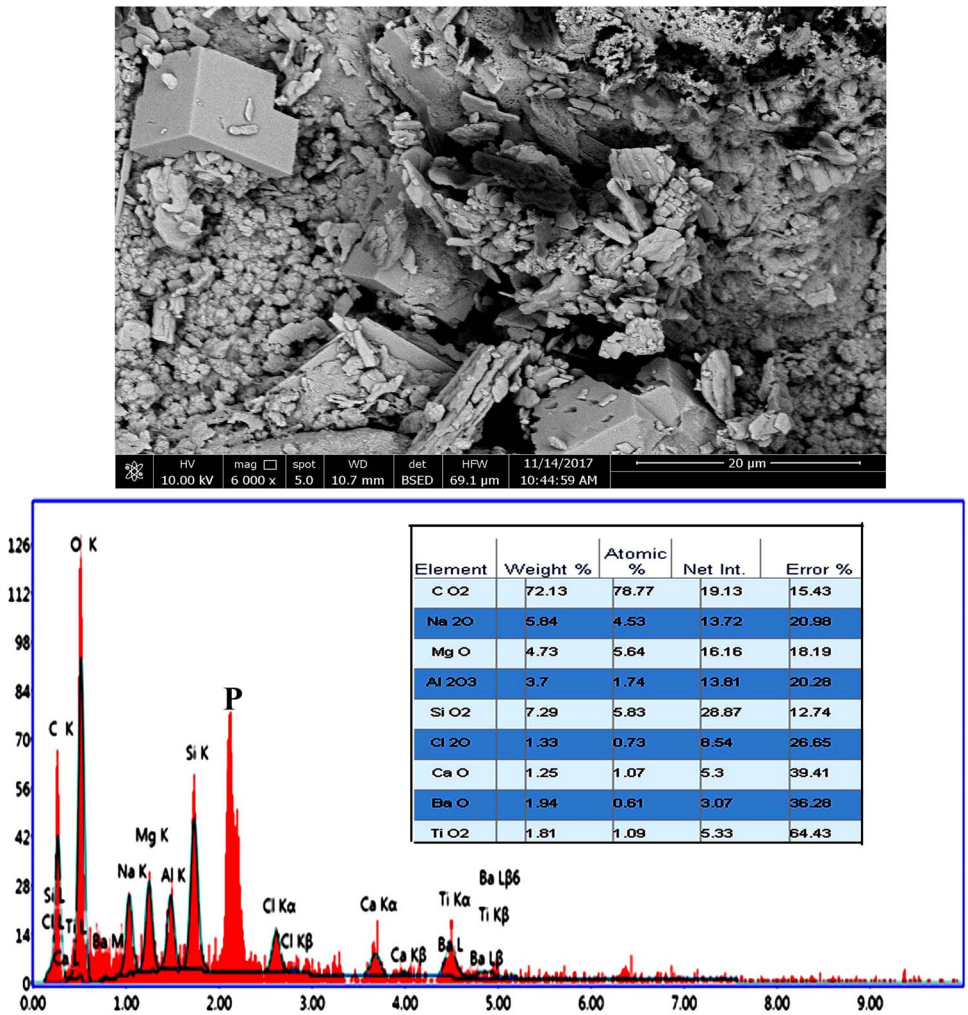

Element	Weight %	Atomic %	Net Int.	Error %
C O2	72.13	78.77	19.13	15.43
Na 2O	5.84	4.53	13.72	20.98
Mg O	4.73	5.64	16.16	18.19
Al 2O3	3.7	1.74	13.81	20.28
Si O2	7.29	5.83	28.87	12.74
Cl 2O	1.33	0.73	8.54	26.65
Ca O	1.25	1.07	5.3	39.41
Ba O	1.94	0.61	3.07	36.28
Ti O2	1.81	1.09	5.33	64.43

Fig. 7 BSE image and EDX analysis data showing rhombohedral crystals and halite crystals are scattered in phosphatic matrix, where content of Mg, Si, Na, Cl, Ba and Ti reach to 4.7, 7.3, 5.8, 1.3, 1.9 and 1.8%; respectively at the dahllite layer of the studied Hamadat Mines

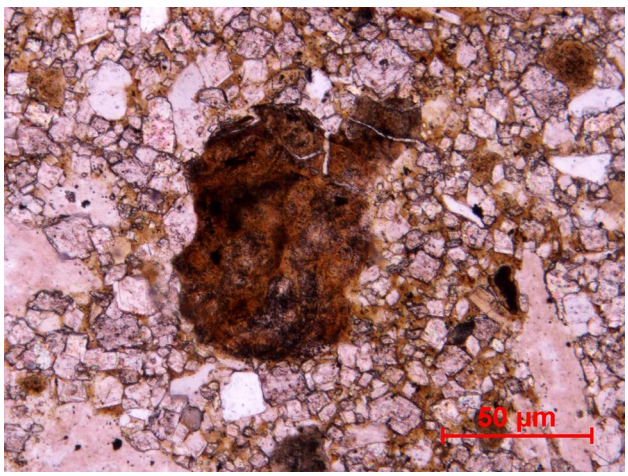

Fig. 8 Assemblage of calcite, dolomite (iron-stained rhombohedral crystals), opaques, and quartz (colourless) associating collophane. Collophane (brown grains, pellets, spheroids, ovoids) is growing at the expense of carbonates. Notice that the boundaries of collophane are convex towards carbonates. PPL

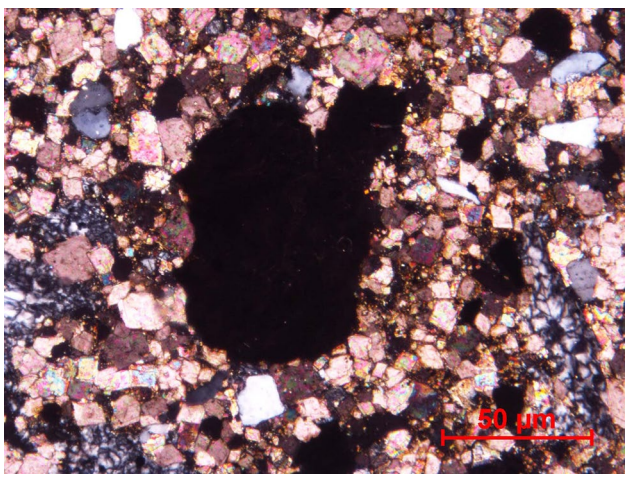

Fig. 9 Assemblage of calcite, dolomite (pastel pink, green, and creamy white interference colours), opaques, and quartz (gray or white interference colours) associating collophane. Collophane (isotropic grains, pellets, spheroids, ovoids) is growing at the expense of carbonates. Notice that the boundaries of collophane are convex towards carbonates. C.N

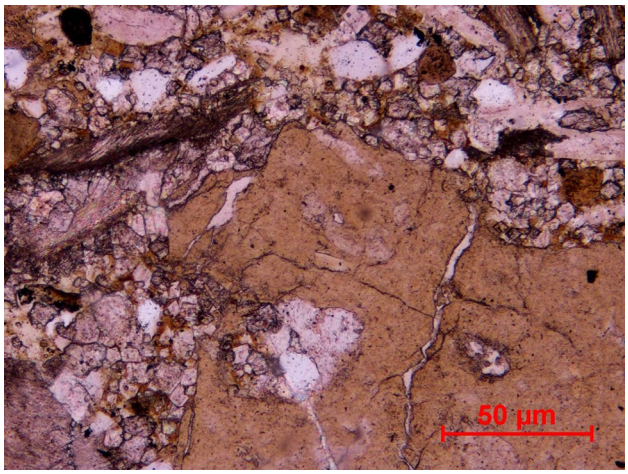

Fig. 10 Assemblage of calcite, dolomite (iron-stained rhombohedral crystals), few magnesite, opaques, and quartz (colourless) associating collophane. Collophane (brown grains, pellets, spheroids, ovoids) is growing at the expense of carbonates. Collophane encloses some rock fragments of carbonates. Notice that the boundaries of collophane are convex towards carbonates. PPL

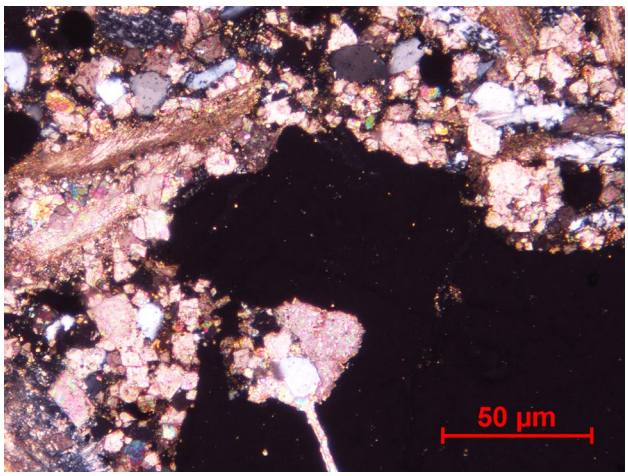

Fig. 11 Assemblage of calcite, dolomite (pastel pink, green, and creamy white interference colours), few magnesite, opaques, and quartz (gray or white interference colours) associating collophane. Collophane (isotropic grains, pellets, spheroids, ovoids) is growing at the expense of carbonates. Collophane encloses some rock fragments of carbonates. Notice that the boundaries of collophane are convex towards carbonates. C.N

Fig. 12 Assemblage of calcite, dolomite (iron-stained rhombohedral crystals), opaques, and quartz (colourless) associating collophane. Collophane (brown grains, pellets, spheroids, ovoids) is growing at the expense of carbonates. Notice that the boundaries of collophane are convex towards carbonates. Lastly, the spherulitic dahllite invading and replacing collophane as well as carbonates, where the spherulitic dahllite is growing at the expense of the collophane as well as carbonates. Spherulitic dahllite structure (colourless to pale brown) exhibits subradiating plumose fibers. PPL

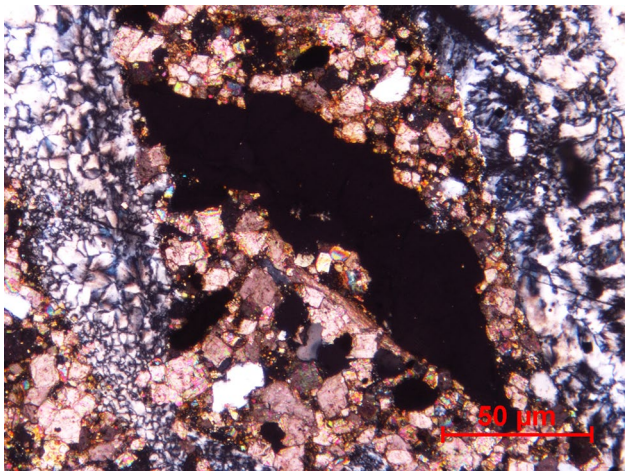

Fig. 13 Assemblage of calcite, dolomite (pastel pink, green, and creamy white interference colours), opaques, and quartz (gray or white interference colours) associating collophane. Collophane (isotropic grains, pellets, spheroids, ovoids) is growing at the expense of carbonates. Notice that the boundaries of collophane are convex towards carbonates. Lastly, the spherulitic dahllite invading and replacing collophane as well as carbonates, where the spherulitic dahllite is growing at the expense of the collophane as well as carbonates. Spherulitic dahllite structure (bluish gray to white interference colours) exhibits subradiating plumose fibers. C.N

may be included and form new crystal lattice. In other case, the re-crystallization of bone fragments and collophanes possibly will incorporate phosphate and/or carbonate ions from ground water.

The obliteration of the organic matrix of bone fragments may assist the dissolution of dahllite crystallites. Therefore, the dahllite crystal size will be increased by the re-crystallization process. This inspection possibly indicates that the chemical composition of the original apatite change gradually during diagenesis. Thus, dahllite is developed as authigenic in the phosphatic rocks. A reason as by authigenic dahllite is developed as a secondary

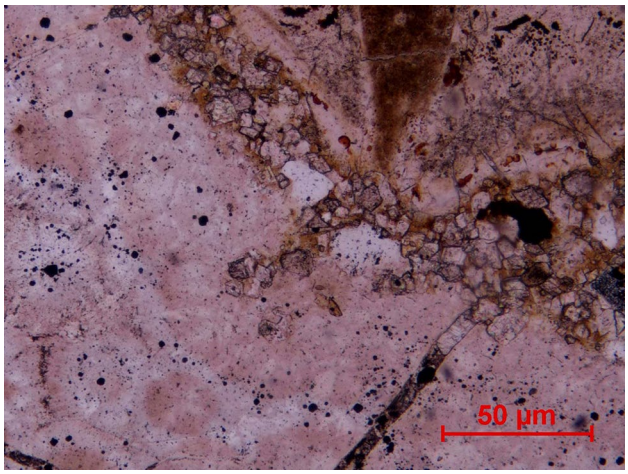

Fig. 14 Assemblage of calcite, dolomite (iron-stained rhombohedral crystals), opaques, and quartz (colourless) associating collophane. Collophane (brown grains, pellets, spheroids, ovoids) is growing at the expense of carbonates. Notice that the boundaries of collophane are convex towards carbonates. Lastly, the spherulitic dahllite invading and replacing collophane as well as carbonates, where the spherulitic dahllite is growing at the expense of the collophane as well as carbonates. Spherulitic dahllite structure (colourless to pale brown) exhibits subradiating plumose fibers. PPL

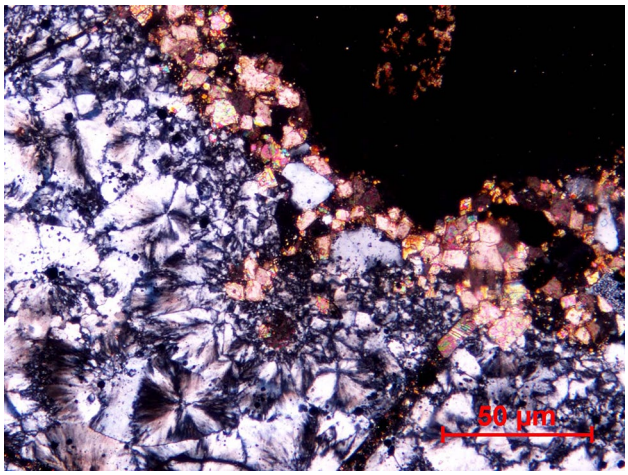

Fig. 15 Assemblage of calcite, dolomite (pastel pink, green, and creamy white interference colours), opaques, and quartz (gray or white interference colours) associating collophane. Collophane (isotropic grains, pellets, spheroids, ovoids) is growing at the expense of carbonates. Notice that the boundaries of collophane are convex towards carbonates. Lastly, the spherulitic dahllite invading and replacing collophane as well as carbonates, where the spherulitic dahllite is growing at the expense of the collophane as well as carbonates. Spherulitic dahllite structure (bluish gray to white interference colours) exhibits subradiating plumose fibers. C.N

mineral at Duwi Format ion at Qusier–Safaga area. In contrast, Ahmad et al. (2019) mentioned that the Upper Campanian-Lower Mastication phosphorite for Central Jordan were represented as reworked origin resulting their

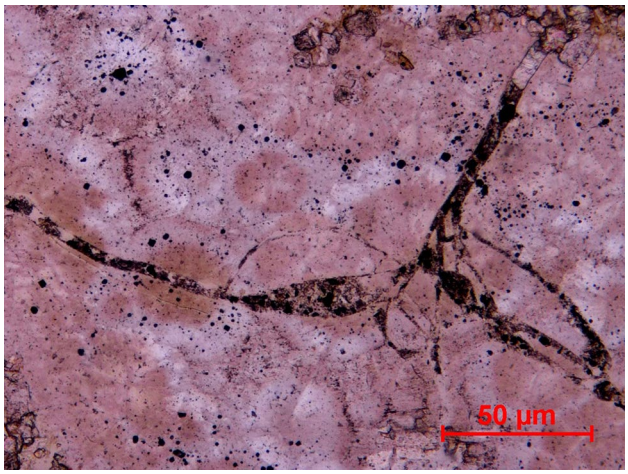

Fig. 16 Lastly, the spherulitic dahllite invading and replacing collophane and carbonates, where the spherulitic dahllite is growing at the expense of the collophane as well as carbonates. Spherulitic dahllite structure (colourless to pale brown) exhibits subradiating plumose fibers. PPL. X40

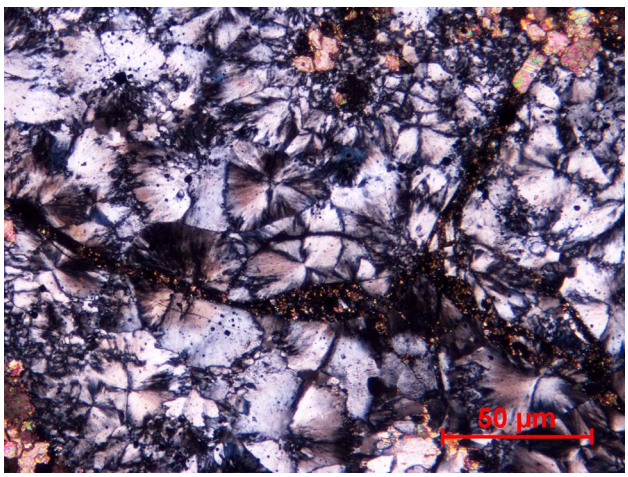

Fig. 17 Lastly, the spherulitic dahllite invading and replacing collophane as well as carbonates, where the spherulitic dahllite is growing at the expense of the collophane as well as carbonates. Spherulitic dahllite structure (bluish gray to white interference colours) exhibits subradiating plumose fibers. C.N

homogeneous texture with lack of any concentric structure in the phosphatic pellets as well as existence of bone remains inside them, which are filled with phosphatic mud like the matrix.

Consequently, the authigenic dahllite in the studied rocks was formed by addition of calcium ions through the re-crystallization of the fluro-apatite (cf. Abou El-Anwar et al. 2019a). On the other hand, collophane and bone fragments re-crystallized may have added ions of Ca or Mg to the phosphate and carbonate rocks. Hence, authigenic dahllite was formed as a secondary mineral (Figs. 6, 11, 16 and 18).

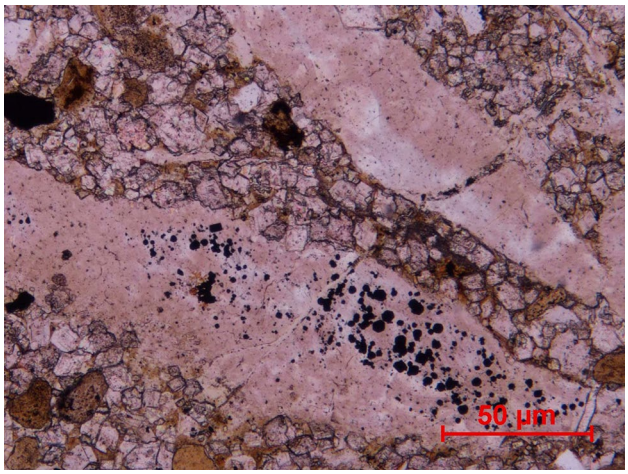

Fig. 18 Lastly, the spherulitic dahllite invading and replacing collophane as well as carbonates, where the spherulitic dahllite is growing at the expense of the collophane as well as carbonates. Spherulitic dahllite structure (colourless to pale brown) exhibits subradiating plumose fibers. Notice: Framboidal pyrite scattered in the matrix and some filled the minor fracture. PPL. X40

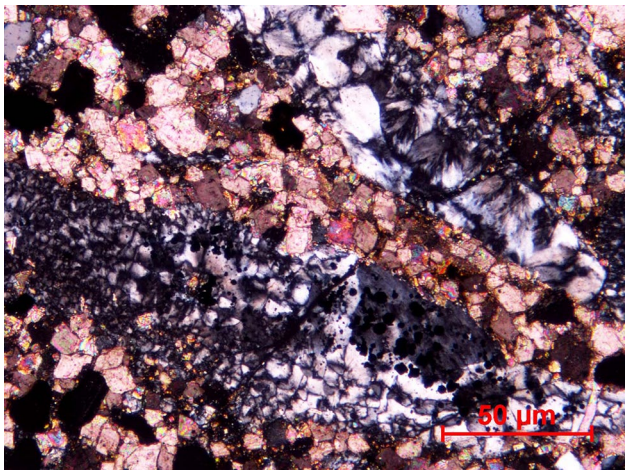

Fig. 19 Lastly, the spherulitic dahllite invading and replacing collophane as well as carbonates, where the spherulitic dahllite is growing at the expense of the collophane as well as carbonates. Spherulitic dahllite structure (bluish gray to white interference colours) exhibits subradiating plumose fibers. Notice: fracture filling with the spherulitic dahllite. C.N

Geochemistry

The results of chemical analysis of major, trace and rare earth elements of representative samples, along with their ratios are quoted in Table 1. The interrelationship between major, trace and rare earth elements is given in Table 2.

Major elements

Generally, the major elements are mainly comparable for the studied two layers**.** CaO is the dominant constituent of the studied samples averaging 38.95% (Table 1). CaO is the dominant constituent of the studied phosphate samples averaging 38.8 and 39.1%; for dahllite and phosphatic layer; respectively, Table 1. SiO_2 is the second abundant elements averaging 21.6 and 18.92% for dahllite and phosphatic layer, respectively, which indicated the presence of quartz grains, conforming with XRD. P_2O_5 content of dahllite and phosphatic layer are 3.96 and 4.11%; respectively. The average of MgO and Fe_2O_3 (2.19 and 1.76%; respectively) for Dahllite layer are higher than those (0.93 and 1.34%; respectively) for phosphatic layer, this revealed that the dahllite layer was abundant in dolomite and pyrite crystals (Table 1), which conformed with XRD and SEM and EDX analysis. Positive correlation between CaO and P_2O_5 ($r=0.66$), suggested that apatite is a moderate control on the phosphate content in these layers (Table 2). Strong positive relation between Ca and Mg ($r=0.67$) reveled the abundance of dolomite, which conformed with XRD and SEM and EDX analyses. The positive correlation between P_2O_5 and Fe_2O_3 ($r=0.45$) revealed that the iron oxides have a high capability for the sorption of phosphate in anoxic environment affected by the aerobic benthic bacteria (cf. Abou El-Anwar et al. 2014 and 2019b). The moderate positive correlation between Sr and Fe_2O_3 ($r=0.46$) indicates that the studied samples were deposited under control of bacterial activity (Table 2), which conformed with the petrographic study [(cf. Abou El-Anwar (2005, 2006, 2011, 2012, 2014 and 2017); and Abou El-Anwar et al. 2014 and 2017)].

Distribution of trace elements and the redox conditions

The values of Sr, Mo, Ni, Zn, Cd and Pd in the studied samples were relatively higher than those of Upper Continental Crust (UCC) and those of the Post Archaean Australian Shale (PAAS), (Taylor and McLennan 1985 and Rudnick and Gao 2003; respectively), Fig. 20.

Dahllite layer has relatively higher content of trace elements than those in the phosphate layer (1864 and 1683 ppm; respectively), averaging 533 and 323 ppm; respectively. This may be a resulting of higher content in SiO_2, Mg and Fe (21.6, 2.19 and 1.76%; respectively) for Dahllite layer than those for phosphate layer (18.92, 0.93 and 1.1%; respectively), (Table 1).

Positive strong to moderate correlation between most of the trace elements (Ni, Zn, V, Cd, Zr, Cr and Rb) with P_2O_5, Al_2O_3 and Mg, indicated that these trace elements may by associated with apatite, clay and dolomite minerals. Most trace elements (Mo, Ni, V, Cd, Zr, Cr, Rb, Ba and Pd) are

Table 1 Chemical analysis of major (%), trace and rare earth elements (ppm) with their ratios and CIA

S. No	15	12	10	9	8	5	3	1	Min	Max	Average
P_2O_5	3.31	3.42	3.84	5.25	3.78	3.81	4.85	3.98	3.31	5.25	4.03
SiO_2	22.6	21.54	20.87	21.4	18.44	19.65	20.24	17.35	17.35	22.6	20.26
Al_2O_3	0.94	0.85	1.01	1.55	1.19	1.23	1.5	1.42	0.85	1.55	1.21
CaO	37.65	38.98	39.24	39.19	38.61	38.82	39.91	39.21	37.65	39.91	38.95
MgO	1.93	2.21	2.51	2.09	0.88	1.05	0.95	0.84	0.84	2.51	1.56
Fe_2O_3	1.47	1.94	1.97	1.65	1.18	1.08	1.12	1.02	1.02	1.97	1.43
Na_2O	0.34	0.32	0.38	0.42	0.32	0.38	0.4	0.38	0.32	0.42	0.37
K_2O	0.08	0.07	0.08	0.01	0.07	0.08	0.05	0.06	0.01	0.08	0.06
SO_3	0.95	0.89	0.92	1.5	1.06	1.45	1.36	1.41	0.89	1.5	1.19
Cl	0.31	0.21	0.25	0.28	0.29	0.3	0.23	0.18	0.18	0.31	0.26
L.O.I	30.7	32.5	30.81	28.51	32.29	30.2	29.52	32.65	28.51	32.65	30.90
Mn	953	840	810	850	620	610	640	685	610	953	751
Sr	601	630	700	778	575	410	270	310	270	778	534
Mo	2	3	4	5	2	3	4	2	2	5	3
Ti	77	80	75	88	70	90	65	78	65	90	77.88
Ba	20	19	35	40	450	350	200	190	19	450	163
Ni	40	38	35	53	55	60	64	58	35	64	50
Zn	80	74	70	85	90	65	87	95	65	95	81
V	20	13	30	100	88	90	70	80	13	100	61
Cd	0.2	0.5	0.9	0.7	0.4	0.6	0.5	0.8	0.2	0.9	1
Pb	0.7	0.9	1	0.8	1.1	0.9	0.88	1.4	0.7	1.4	1
Co	2.5	3	2.7	2.8	4	3	2.5	3.1	2.5	4	3
Zr	17	20	25	27	27	29	30	32	17	32	26
Cr	24	22	30	27	20	17	12	20	12	30	22
Rb	1	2	1	9	7	8	9	7	1	9	6
Y	7.7	3	5	12	5	8	7	6	3	12	7
La	2	5	2	3	4	4	5	3	2	5	4
Pr	25	30	22	25	34	33	37	35	22	37	30
Se	0.1	0.1	0.2	0.1	0.3	0.1	0.1	0.2	0.1	0.3	0.15
Sc	28.2	25	23.5	10.4	20.5	19.6	20.1	15.3	10.4	28.2	20
I	7.1	5.2	3.4	2.1	6.5	4.3	7.5	2.4	2.1	7.5	5
Hf	2	1.7	0.9	0.7	0.4	0.5	0.4	0.3	0.3	2	1
Ce	4.1	4.5	3.8	4.1	5.1	7.2	6.4	5.8	3.8	7.2	5
Cs	40	35	33	37	15	18	21	20	15	40	27
Ag	0.1	0.1	0.2	0.1	0.1	0.1	0.2	0.1	0.1	0.2	0.13
Ta	4.1	3.4	4.5	3.5	3.8	2.4	3.7	2.9	2.4	4.5	4
Nd	2.4	1.9	2.1	2.8	1.7	1.5	1.6	1.3	1.3	2.8	2
Ti	4.8	4.5	4.8	4.1	4.6	2.4	2.5	3.5	2.4	4.8	4
W	10.3	8.5	8.9	9.4	7.6	4.9	5.4	3.7	3.7	10.3	7
U	1.9	3.1	2.8	2.3	0.9	1.9	1.4	1.9	0.9	3.1	2
Th	4.8	4.9	4.1	4.8	3.1	2.7	3.1	2.9	2.7	4.9	4
V/Ni	0.50	0.34	0.86	1.89	1.60	1.50	1.09	1.38	0.37	1.56	1.22
V/Cr	0.83	0.59	1.00	3.70	4.40	5.29	5.83	4.00	1.08	3.33	2.85
Ni/Co	16.0	12.7	13.0	18.9	13.8	20.0	25.6	18.7	14.0	16.0	17.1
V/Mo	10.0	4.3	7.5	20.0	44.0	30.0	17.5	40.0	6.5	20.0	19.6
Th/U	2.53	1.58	1.46	2.09	3.44	1.42	2.21	1.53	3.00	1.58	1.88
U/Th	0.40	0.63	0.68	0.48	0.29	0.70	0.45	0.66	0.33	0.63	0.53
La/Ce	0.05	0.14	0.06	0.08	0.27	0.22	0.24	0.15	0.13	0.13	0.13
CIA	55.29	54.49	54.59	64.58	62.63	59.42	63.83	63.39	56.67	62.75	60.30
trace	1837.4	1743.4	1818.6	2057.3	2002.5	1728.5	1445.88	1555.3	1111.4	2603.3	1773.61
ΣREE	145.6	137.9	122.2	130.4	119.6	118.6	131.4	111.3	73.2	178.8	127.13

Table 1 (continued)

S. No	15	12	10	9	8	5	3	1	Min	Max	Average
ΣLREE	32.6	31.9	27.6	16.2	26.2	25.1	26.7	19.6	13.7	36	25.7375
ΣHREE	35.9	28	28.5	22.4	25.5	27.6	27.1	21.3	13.4	40.2	27.0375

highly to moderate positive correlating with Mg ($r=0.57$, 0.71, 0.78, 0.57, 0.81, 0.62, 0.79, 0.21 and 0.15; respectively), which indicated the vital role of the dolomitization process in the concentration of these elements in the studied samples (Table 2).

The content of some elements, such as Pb, Zn, Cu, Ni, Cd, Mo, and Ba, and low content of Co in the studied samples provides evidence of the genetic role of hydrothermal solutions in Hamadat Mines (cf. Nicholson 1992).

V/Cr (2.85) higher than 2.0 (Table 1) indicate that the phosphatic rocks in Hamadat Mines in the stage of late stage diagenesis (Trueman and Tuross 2002), which conformed with mineralogically and petographically studies.

Trace elements and the ratio of U/Th, V/Cr, Ni/Co and authigenic uranium can be indicating the redox conditions of rocks. U/Th > 1.25 indicates an anoxic environment, and 0.75–1.25 sign a suboxic to dysoxic environment, while a < 0.75 indicates an oxic environment (Jones and Manning 1994). V/Cr > 4.25 denoting an anoxic environment, range from 2.0 to 4.25 indicates a suboxic to dysoxic environment, while a < 2.0 suggests an oxic environment. Ni/Co > 7.0 indicate anoxic, from 5.0 to 7.0 declares suboxic to dysoxic and lower than 5.0 point to anoxic environment. U content higher than 12 indicates anoxic conditions, range from 5 to 12.0 indicates suboxic to dysoxic conditions, while the < 5.0 indicates oxic conditions. Table 1 shows the values of U/Th (0.53) and U average content (2.0) indicated oxic condition. Meanwhile, V/Ni (1.22), Ni/Co (17.1), V/Cr (2.85) indicated an anoxic condition (Jones and Manning 1994 and Shi et al. 2015). In addition, Th/U was recorded 1.88 indicating mainly anoxic environment (Pi et al. 2014). Thus, the results declare and pointed to the oxic to anoxic environment in which the studied phosphatic rocks are deposited (cf. Abou El-Anwar 2019).

Mobilization and Re-distribution of rare earth elements

Br, Sc, Se, I, Cs, Ta, Ti and W concentrations in the studied phosphatic rocks were higher than those reported by Taylor and McLennan (1985) for Upper Continental Crust (UCC) and those of the Post Archaean Australian Shale (PAAS) recorded by Rudnick and Gao (2003), Fig. 21. The percentages of Mn, Ba, Br and Nb were lower than those of (UCC) and (PAAS).

Dahllite layer have relatively higher in rare earth elements than those in the phosphate layer (134 and 120 ppm; respectively), Table 1 and Fig. 21. Rare earth elements (Y, Nd, W, Cs, Ti and Ta) are in highly to moderate positive correlation with Fe ($r=0.84$, 0.77, 0.51, 0.46, 0.18, and 0.16; respectively), (Table 2). Strong to moderate positive relation between SiO_2 and Hf, W, Nd, Ta, Sc, Ti, Cs and I ($r=0.81$, 0.81, 0.77, 0.47, 0.44, 0.37, 0.26 and 0.24; respectively). Mg positive correlation with Y, Ce and Pr ($r=0.6$, 0.56 and 0.3; respectively). Thus, Fe and Mn oxides and terrigenous clastic could concentrate and control the distribution of certain rare earth metals in the phosphatic rocks at Hamadat Mines. Fe and Mg oxyhydroxides were adsorptive scavenging the trace elements in the studied rock samples under anoxic condition according to Sholkovitz et al. (1992).

The results show that was comparable to light rare earth elements (LREE, 25.74 ppm) content in the studied samples and that of heavy rare earth elements (HREE, 27.04 ppm), (Table 1). These values are very lower than to those in UCC (Rudnick and Gao 2003) and PAAS (Taylor and McLennan 1985) 535 and 414 ppm; respectively.

Hydrothermal crusts have La/Ce (~2.8) ratios indicating sea water origin, while hydrogenous Mn–Fe crusts have a much lower La/Ce ratio (~0.25), Nath et al. (1997). The average of La/Ce ratios in the bulk samples from the studied phasphatic rocks is 0.13, which supported the major elements were mainly of hydrogenous origin (Table 1).

REEs (La, Br, I, Ce, Y and Nd) have a moderate to low positive correlation with Th ($r=0.68$, 0.67, 0.57, 0.35, 0.26 and 0.17; respectively) reveled that monazite grains occurred in the studied phosphatic rocks, whereas REE substitutes Ca in the phosphatic lattice (Table 2). The strong positive correlation between U and Th ($r=0.75$) in the studied rocks indicated the incorporation of U and Th in rare-earth phosphates, in exacting monazite. Thus, they are acting as matrices for immobilization of nuclear waste.

Modern phosphates are low in REEs and reflect the characteristic pattern of modern seawater. Consequently, REEs can be fractionated during their absorption into francolite from seawater, which explain the low content of REEs in the studied rocks and which is in agreement with Lécuyer et al. (2004).

Thus, the rare earth elements in the studied phosphorites at Hamadat Mines may be derived either directly or indirect from sea water, by remobilization and associated with clastic materials and/or the ferromanganese oxides.

Table 2 Correlation coefficients between major, trace and rare earth elements

	P2O5	SiO2	Al2O3	TiO2	CaO	MgO	Fe2O3	Na2O	K2O	SO3	Cl	L.O.I.	Mn	Sr	Mo	Ba	Ni	Zn	V	Cd	Pb
P2O5	1.00																				
SiO2	-0.06	1.00																			
Al2O3	0.88	0.44	1.00																		
TiO2	0.02	0.17	0.01	1.00																	
CaO	0.66	-0.33	0.58	-0.22	1.00																
MgO	0.77	-0.34	0.84	0.34	0.67	1.00															
Fe2O3	0.45	0.43	0.34	0.28	-0.36	0.10	1.00														
Na2O	0.83	-0.04	0.78	0.24	0.59	0.88	0.31	1.00													
K2O	-0.89	-0.05	-0.75	-0.19	-0.44	-0.57	-0.61	-0.64	1.00												
SO3	0.72	-0.42	0.90	0.36	0.45	0.92	0.29	0.76	-0.61	1.00											
Cl	-0.07	0.40	-0.14	0.26	-0.61	-0.14	0.59	-0.08	0.10	-0.05	1.00										
L.O.I.	-0.73	-0.46	-0.50	-0.25	-0.23	-0.57	-0.63	-0.76	0.58	-0.50	-0.45	1.00									
Mn	-0.19	0.81	-0.47	0.21	-0.48	-0.49	0.45	-0.11	-0.09	-0.48	0.15	-0.14	1.00								
Sr	0.28	0.55	-0.10	0.23	-0.07	-0.04	0.46	0.08	-0.32	-0.18	0.58	-0.51	0.32	1.00							
Mo	0.77	0.39	0.41	0.20	0.61	0.57	0.27	0.73	-0.65	0.32	0.01	-0.78	0.14	0.61	1.00						
Ba	-0.02	-0.72	0.29	-0.16	0.05	0.21	-0.22	-0.16	0.20	0.32	0.22	0.21	-0.88	-0.18	-0.39	1.00					
Ni	0.55	-0.62	0.82	-0.06	0.43	0.71	0.07	0.44	-0.36	0.84	-0.05	-0.24	-0.78	-0.34	0.02	0.68	1.00				
Zn	0.35	-0.48	0.55	-0.46	0.15	0.06	0.25	0.07	-0.46	0.28	-0.35	0.19	-0.17	-0.37	-0.23	0.19	0.44	1.00			
V	0.67	-0.66	0.91	0.11	0.43	0.78	0.22	0.56	-0.54	0.89	0.01	-0.30	-0.69	-0.12	0.16	0.63	0.90	0.48	1.00		
Cd	0.35	-0.36	0.33	0.24	0.64	0.57	-0.34	0.58	-0.23	0.31	-0.49	-0.06	-0.19	-0.01	0.46	-0.13	0.02	-0.09	0.27	1.00	
Pb	-0.09	-0.90	0.24	-0.19	0.32	0.15	-0.54	-0.04	0.11	0.18	-0.64	0.65	-0.53	-0.60	-0.40	0.40	0.28	0.48	0.38	0.51	1.00
Co	-0.22	-0.63	-0.02	-0.08	-0.13	-0.18	-0.19	-0.51	0.13	-0.06	0.06	0.57	-0.51	0.04	-0.46	0.73	0.21	0.29	0.33	-0.07	0.52
Zr	0.57	-0.80	0.81	-0.05	0.70	0.81	-0.22	0.58	-0.33	0.77	-0.35	-0.11	-0.81	-0.32	0.18	0.56	0.81	0.36	0.87	0.57	0.63
Cr	0.43	-0.50	0.62	-0.18	0.62	0.62	-0.23	0.69	-0.20	0.54	-0.55	-0.13	-0.35	-0.55	0.18	0.00	0.44	0.34	0.46	0.64	0.55
Rb	0.68	-0.56	0.87	0.23	0.41	0.79	0.26	0.52	-0.61	0.90	0.03	-0.34	-0.65	-0.03	0.22	0.59	0.89	0.39	0.97	0.18	0.25
Y	0.69	0.21	0.64	0.47	-0.01	0.60	0.84	0.72	-0.69	0.70	0.46	-0.83	0.14	0.33	0.50	-0.10	0.38	0.11	0.53	0.04	-0.40
La	0.15	-0.20	0.15	-0.19	0.46	0.18	-0.37	-0.16	-0.10	0.17	-0.30	0.11	-0.54	-0.11	0.05	0.38	0.46	0.05	0.21	-0.21	0.01
Pr	0.11	-0.69	0.42	-0.33	0.37	0.30	-0.37	-0.06	0.02	0.43	-0.35	0.28	-0.81	-0.61	-0.35	0.70	0.80	0.43	0.55	-0.16	0.46
Se	-0.21	-0.65	-0.03	-0.42	-0.04	-0.26	-0.27	-0.36	0.24	-0.23	-0.06	0.56	-0.40	-0.05	-0.42	0.54	0.03	0.40	0.20	0.17	0.67
Sc	-0.80	0.44	-0.87	-0.35	-0.51	-0.81	-0.33	-0.70	0.81	-0.84	0.17	0.37	0.33	-0.08	-0.45	-0.19	-0.60	-0.43	-0.84	-0.53	-0.33
I	-0.29	0.24	-0.30	-0.64	-0.27	-0.50	-0.04	-0.50	0.39	-0.40	0.29	0.07	-0.08	-0.07	-0.35	0.23	0.04	0.04	-0.29	-0.83	-0.40
Hf	-0.56	0.81	-0.78	0.11	-0.64	-0.73	0.17	-0.50	0.31	-0.70	0.20	0.11	0.85	0.17	-0.17	-0.67	-0.79	-0.36	-0.88	-0.51	-0.59
Ce	0.12	-0.56	0.43	0.03	0.33	0.56	-0.34	0.20	0.13	0.61	-0.09	-0.02	-0.83	-0.52	-0.18	0.68	0.82	-0.01	0.58	-0.01	0.26
Cs	-0.43	0.26	-0.45	0.38	-0.84	-0.53	0.46	-0.52	0.15	-0.36	0.66	0.16	0.41	0.45	-0.35	0.04	-0.41	-0.13	-0.23	-0.42	-0.26
Ag	0.29	0.10	0.10	-0.58	0.59	0.16	-0.33	0.38	0.06	-0.12	-0.22	-0.30	-0.12	0.08	0.48	-0.17	-0.05	-0.13	-0.12	0.34	-0.06
Ta	-0.06	0.47	-0.35	-0.57	-0.14	-0.55	0.16	-0.17	0.08	-0.67	0.15	-0.07	0.51	0.42	0.17	-0.43	-0.61	0.05	-0.53	-0.12	-0.28
Nd	0.26	0.77	-0.09	0.29	-0.31	-0.16	0.77	0.18	-0.46	-0.17	0.47	-0.55	0.79	0.75	0.50	-0.63	-0.50	-0.13	-0.28	-0.12	-0.68
Ti	-0.41	0.37	-0.60	-0.10	-0.52	-0.77	0.18	-0.52	0.14	-0.76	0.14	0.33	0.68	0.40	-0.17	-0.43	-0.82	0.03	-0.62	-0.13	-0.10
W	-0.14	0.81	-0.50	0.07	-0.50	-0.58	0.51	-0.26	-0.07	-0.60	0.48	-0.22	0.82	0.72	0.22	-0.58	-0.76	-0.24	-0.61	-0.32	-0.66
U	0.69	0.04	0.54	-0.31	0.45	0.28	0.34	0.22	-0.69	0.33	-0.03	-0.39	-0.22	0.28	0.43	0.15	0.49	0.46	0.42	-0.25	-0.24
Th	0.18	-0.13	0.28	-0.28	-0.02	-0.03	0.23	-0.25	-0.28	0.21	0.05	0.04	-0.30	-0.13	-0.23	0.41	0.54	0.51	0.33	-0.67	-0.11

	Co	Zr	Cr	Rb	Y	La	Pr	Se	Sc	I	Hf	Ce	Cs	Ag	Ta	Nd	Ti	W	U	Th
Co	1.00																			
Zr	0.24	1.00																		
Cr	-0.32	0.73	1.00																	
Rb	0.33	0.79	0.30	1.00																
Y	-0.33	0.20	0.15	0.55	1.00															
La	0.25	0.25	-0.16	0.36	-0.29	1.00														
Pr	0.37	0.61	0.28	0.57	-0.21	0.73	1.00													
Se	0.79	0.28	0.04	0.06	-0.41	-0.16	0.15	1.00												
Sc	-0.17	-0.73	-0.45	-0.85	-0.62	-0.06	-0.20	-0.05	1.00											
I	-0.01	-0.37	-0.38	-0.27	-0.31	0.37	0.31	-0.04	0.66	1.00										
Hf	-0.39	-0.97	-0.61	-0.80	-0.19	-0.23	-0.57	-0.43	0.70	0.30	1.00									
Ce	0.13	0.65	0.36	0.60	0.03	0.55	0.83	-0.11	-0.21	0.15	-0.59	1.00								
Cs	0.43	-0.57	-0.76	-0.18	0.11	-0.39	-0.46	0.23	0.19	0.00	0.44	-0.47	1.00							
Ag	-0.45	0.20	0.47	-0.23	-0.16	0.00	-0.07	0.00	0.16	0.19	-0.20	-0.01	-0.68	1.00						
Ta	-0.20	-0.49	-0.16	-0.63	-0.18	-0.42	-0.58	0.24	0.44	0.31	0.38	-0.76	0.13	0.53	1.00					
Nd	-0.35	-0.56	-0.40	-0.23	0.54	-0.47	-0.81	-0.32	-0.05	-0.15	0.51	-0.77	0.48	-0.08	0.51	1.00				
Ti	0.18	-0.69	-0.50	-0.65	-0.27	-0.51	-0.68	0.36	0.37	-0.03	0.59	-0.92	0.65	-0.16	0.70	0.56	1.00			
W	-0.19	-0.82	-0.65	-0.56	0.12	-0.41	-0.82	-0.12	0.36	0.13	0.72	-0.87	0.62	-0.05	0.70	0.88	0.80	1.00		
U	0.09	0.23	-0.09	0.52	0.28	0.62	0.39	-0.13	-0.40	0.30	-0.27	0.12	-0.24	0.11	0.02	0.15	-0.25	0.00	1.00	
Th	0.32	0.06	-0.30	0.44	0.26	0.68	0.67	-0.06	-0.10	0.57	-0.09	0.35	0.02	-0.34	-0.26	0.17	-0.27	-0.17	0.75	1.00

Paleoclimate

The CIA can be reflecting the paleoclimatic conditions. CIA from 50 to 65, indicated cold and dry climate during low chemical weathering, 65 to 85, it denotes a warm and humid climate during moderate chemical weathering, while a value between 85 and 100 indicated a hot and humid climate during strong chemical weathering (Nesbitt and Young 1982; McLennan 1993). The CIA of the studied phosphatic ranged between 55 and 74 with average 60.3% indicating that these rocks may be deposited in cold and dry climate during low weathering. The immobile elements can be used as markers of provenance such as weathering (Taylor and McLennan 1985). Thus, the strong positive correlations between Al_2O_3 and Ni, Zn, V, Zr, Cr, Rb, Y and U ($r = 0.82$, 0.55, 0.81, 0.81, 0.62, 0.86, 0.64 and 0.54; respectively, Table 2) as well as moderate relation with Cd and La ($r = 0.33$ and 0.15; respectively) reveal that these immobile elements were concentrated during a weathering processes (Fedo et al. 1996).

Conclusion

Petrographical studies, concentrations of trace, rare earth elements and their ratios indicated that the phosphatic rocks at Hamadat Mines were deposited under oxic to anoxic condition. In addition, these phosphatic rocks were of hydrogenous origin formed in cold and dry climate during low weathering. The secondary authigenic dahllite in the Hamadat Mines were formed resulting from the re-crystallization of the fluro-apatite and dolomitization of the carbonate rocks.

The terrigenous clastic input, ferro-manganese oxides and diagensis processes (dolomitization and re-crystallization) are responsible for the relatively high some of trace and most rare earth elements in dahllite layer than phosphatic layer in Hamadat Mines rocks. Thus, dahllite structure may have has the ability to scavenging trace and rare earth elements than the phosphatic structure. The enrichment degree of ΣLREE is relatively lower than that of ΣHREE. Finally, the concentration of trace and rare earth elements reveal that the studied phosphatic rocks of Hamadat Mines have an economic value.

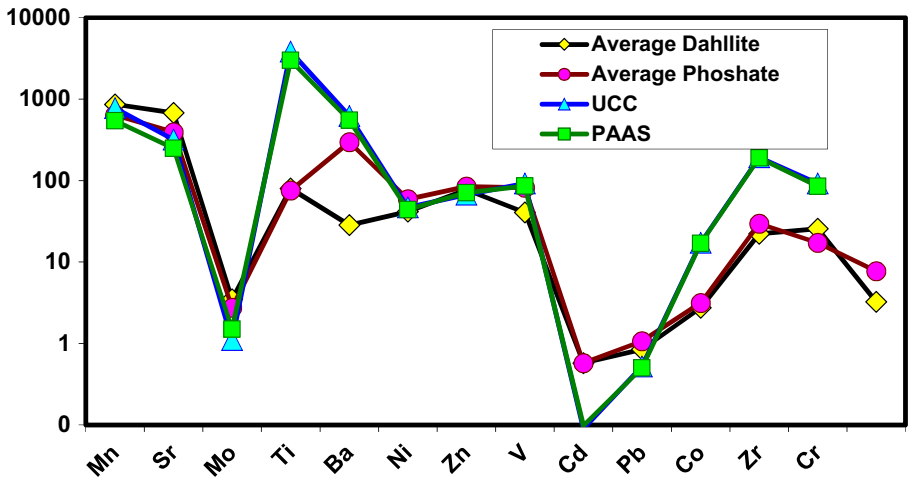

Fig. 20 Concentrations of the trace elements in the studied phosphatic rocks correlated with UCC (Rudnick and Gao 2003) and PAAS (Taylor and McLennan 1985)

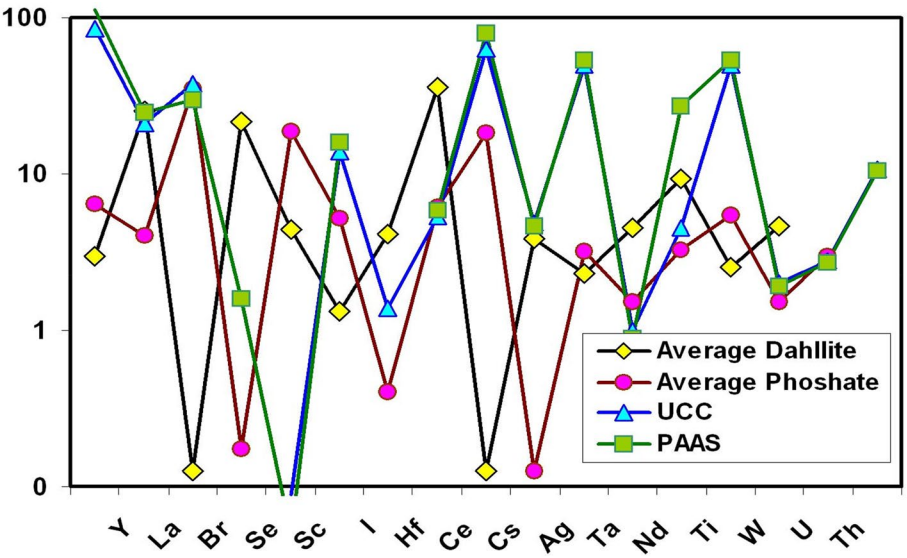

Fig. 21 Concentrations of the trace and rare earth elements in the studied black shales correlated with UCC (Rudnick and Gao 2003) and PAAS (Taylor and McLennan 1985)

References

Abou El-Anwar EA (2005) Petrography, geochemistry and genesis of the Upper Eocene carbonate terraces (II and III), Qasr El-Sagha Formation. El-Faiyum Egypt Sedimentol Egypt 13:243–260

Abou El-Anwar EA (2006) Petrography, geochemistry and genesis of some Middle Eocene rocks at Qattamia area, Cairo-Suez Road Egypt. NRC Egypt 3(6):519–543

Abou El-Anwar EA (2010) Petrographical, geochemical and environmental studies of the subsurface carbonate sediments of el-azima well, western samalut, samalut formation, el-minia Egypt. Sedimentol Egypt 18:98–100

Abou El-Anwar EA (2011) Petrographical, geochemical and diagenetic studies of the middle eocene carbonates, mokattam formation of darb el-fayium area. (Int. Conf. on geological sciences and engineering, France. Paris. Augustus 80:1315–1325

Abou El-Anwar EA (2012) Contribution to the composition and origin of the reef terraces in Ras Mohamed, Sharm El-Sheikh Coast, Southern Sinai. Egypt Egyp J of Geol 56:33–48

Abou El-Anwar EA (2014) Composition and origin of the dolostones of um bogma formation lower carboniferous, west central Sinai, Egypt. Carbonates Evaporates 29:129–205. https://doi.org/10.1007/s13146-014-0188-3

Abou El-Anwar EA (2017) Mineralogical, petrographical, geochemical, diageneses and provenance of the cretaceous black shales duwi formation at Quseir-Safaga, Red Sea, Egypt, Egyptian. J Pet 26:915–926

Abou El-Anwar EA (2019) Lithologic characterization of the phosphorite-bearing Duwi Formation (Campanian), South Esna, West Nile Valley, Egypt. Carbonates Evaporates 34:793–805. https://doi.org/10.1007/s13146-018-0442-1

Abou El-Anwar EA, Sadek MS (2008) Composition of black shale from Quseir, Red Sea, Egypt with emphasis on the sequential extraction of some metals Bull. NRC Egypt 32(5):511–536

Abou El-Anwar EA, Mekky HS, Samy YM (2014) Contribution to the mineralogical, geochemical and provenance of the Cretaceous black shales, Duwi formation, Quseir- Safaga, Red Sea Coast Egypt. Egypt J Geol 58:303–322

Abou El-Anwar EA, Mekky HS, Abd El Rahim SH, Aita SK (2017) Mineralogical, geochemical characteristics and origin of Late Cretaceous phosphorite in Duwi formation (Geble Duwi Mine) Red Sea region, Egypt, Egyptian. J Pet 26:157–169

Abou El-Anwar EA, Abd El Rahim SH, Mekky HS (2019a) Spherulitic dahllite of Duwi formation phosphorite. Carbonates Evaporites 34:557–562. https://doi.org/10.1007/s13146-017-0377-y

Abou El-Anwar EA, Mekky HS, Abdel Wahab W (2019b) Geochemistry, mineralogy and depositional environment of black shales of the Duwi formation Qusseir area, Red Sea coast, Egypt. Carbonates Evaporites 34:883–892. https://doi.org/10.1007/s13146-017-0417-7

Ahmad F, Baioumy H, Farouk S, Al-Kahtany K, El-Sorogy A, Kirk J (2019) Geochemistry and stable isotopes of the upper Campanian-lower Maastrichtian phosphorite-bearing sequence, Central Jordan: implication s for their age, origin, and diagenesis. Geol J. https://doi.org/10.1002/gj.3692

Baioumy H, Tada R (2005) Origin of Late Cretaceous phosphorites in Egypt. Cretac Res 26:261–275

Dorozhkin SV (2010) Nanosized and nanocrystalline calcium orthophosphates. Acta Biomater 6:715–734

Eitel W (1924) Über Karbonatphosphate der Apatitgruppe. Schr. königsb. gelehrt. Ges., naturw. Kl.1:159–177

Fedo CM, Eriksson K, Krogstad EJ (1996) Geochemistry of shale from the Archean (~ 3.0 Ga) Buhwa greenstone belt, Zimbabwe: implications for provenance and source area weathering. Geochem Cosmic Acta 60(10):1751–1763

Germann K, Bock WD, Ganz H, Schröter T, Tröger U (1987) Depositional conditions of Late Cretaceous phosphorites and blackshales in Egypt. Berliner geowiss Abh 75(3):629–668

Jones B, Manning DA (1994) Comparison of geochemical indices used for the interpretation of palaeoredox conditions in ancient mudstones. Chem Geol 111:111–129

Lacroix A (1910) Sur la constitution mineralogique des phosphorites francais. Compt rend 150:1213–1217. Lacroix Mineralogie France 4:555–558

Loukina S, Abou El-Anwar EA (1991) Petrography, mineralogy and diagenesis of Gebel ataqa dolostones. EgyptJ Geol 35(1–2):133–145

Lécuyer C, Reynard B, Grandjean P (2004) Rare earth element evolution of Phanerozoic seawater recorded in biogenic apatites. Chem Geol 204:63–102

McLennan SM (1993) Weathering and global denudation. J Geol 101(2):295–303

Nath BB, Pluger WL, Roelandts I (1997) Geochemical constraints on the hydrothermal origin of ferromanganese incrustations from the Rodriguez triple junction, Indian Ocean. In: Nicholson K, Hein JR, Bu¨hn B, Dasgupta S (Eds.), Manganese mineralization: geochemistry and mineralogy of terrestrial and marine deposits. Geol Soci Lond Spec Publ 119:199–211

Nesbitt HW, Young GM (1982) Early Proterozoic climates and plate motions inferred from major element chemistry of lutites. Nature 199:715–717

Nicholson K (1992) Contrasting mineralogical–geochemical signatures of manganese oxides: guides to metallogenesis. Econ Geol 87:1253–1264

Nowak GJ (2007) Comparative studies of organic matter, petrography of the late Paleozoic black shales from southwestern Poland. Inter J of Coal Geol 71(4):1–18

Pi DH, Jiang SY, Luo L, Yang JH, Hong-Fei Ling HF (2014) Depositional environments for stratiformwitherite deposits in the lower Cambrian black shale sequence of the Yangtze platform, southern Qinling region, SW China: evidence from redox-sensitive trace element geochemistry. Palaeogeogr Palaeoclimatol Palaeoecol 398:125–131

Rogers AF (1912) Dahllite (podolite) from Tonopah, Nevada, voelckerite a new calcium phosphate; remarks on the chemical composition of apatite and phosphate rock. Am J Sci 33:475–482

Rogers AF (1924) Mineralogy and petrography of fossil bone. Geol Soc Am Bull 35:549

Rogers AF, Kerr PF (1942) Optical mineralogy, 2nd edn. McGraw-Hill Book Company Inc, New York and London, p 390

Rudnick RL, Gao S (2003) Composition of the continental crust. Treat Geochem 3:1–64. https://doi.org/10.1016/B0-08-043751-6/03016-4

Said R (1990) The geology of Egypt. Netherlands, A.A, Balkema, Rotterdam, p 734

Sanz M, Daura J, Eguez N, Cabanes D (2015) On the track of anthropogenic activity in carnivore dens: altered combustion structures in Cova del Gegant (NE Iberian Peninsula). Quat Int 437(part:B):1–13

Schieber J, Baird G (2001) On the origin and significance of pyrite spheres in Devonian black shale of North America. J Sediment Res 71(1):155–166

Sengul H, Ozer AK, Gulaboglu MS (2006) Benefication of Mardin-Mazidagi (Turkey) calcareous phosphate rock using dilute acetic acid solutions. Chem Eng J 122:135–140

Shi C, Cao J, Bao J, Zhu C, Jiang X, Wu M (2015) Source characterization of highly mature pyrobitumens using trace and rare earth element geochemistry: sinian-paleozoic paleo-oil reservoirs in south China. Org Geochem 83–84:77–93

Sholkovitz ER, Shaw TJ, Schneider DL (1992) The geochemistry of rare earth elements in the seasonally anoxicwater column and porewaters of Chesapeake Bay. Geochim Cosmochim Acta 56:3389–3402

Taylor SR, McLennan SM (1985) The continental crust: its composition and evolution. Blackwell, Oxford, 312p

Trueman CN, Tuross N (2002) Trace elements in recent and fossil bone apatite. Rev Mineral Geochem 48(1):489–521